Monte Carlo simulation of semiconductor detector response to 222Rn and 220Rn environments.

J. Irlinger[a,*], S. Trinkl[a], M. Wielunksi[a], J. Tschiersch[a], W. Rühm[a]

[a]*Helmholtz Zentrum München, Institute of Radiation Protection, Ingolstädter Landstraße 1, 85764 Oberschleißheim, Germany*

Abstract

A new electronic radon/thoron exposimeter employing semiconductor detectors based on a passive diffusion chamber design has been recently developed at the Helmholtz Zentrum München (HMGU). This device allows for acquisition of alpha particle energy spectra, in order to distinguish alpha particles originating from radon and radon progeny decays, as well as those originating from thoron and its progeny decays. A Monte-Carlo application is described which uses the Geant4 toolkit to simulate these alpha particle spectra. Reasonable agreement between measured and simulated spectra were obtained for both ^{220}Rn and ^{222}Rn, in the energy range between 1 and 10 MeV. Measured calibration factors could be reproduced by the simulation, given the uncertainties involved in the measurement and simulation. The simulated alpha particle spectra can now be used to interpret spectra measured in mixed radon/thoron atmospheres. The results agreed well with measurements performed in both radon and thoron gas environments. It is concluded that the developed simulation allows for an accurate prediction of calibration factors and alpha particle energy spectra.

Keywords: radiation, radon, thoron, monitor, exposimeter, Monte-Carlo, simulation, spectrometry

1. Introduction

In order to quantify the radon (^{222}Rn) exposure of an individual, a portable electronic radon exposure meter has been developed at the Helmholtz Zentrum München (HMGU) [1, 2]. This device allows for a realistic and on-line evaluation of a persons' radon exposure and, consequently, allows prevention against high exposure when constantly worn. However, despite these efforts to quantify individual radon exposure, the effects of the decay products of another radon isotope, ^{220}Rn, commonly called thoron, have not yet been adequately taken into account. Thoron is considered to contribute about 4% to the annual effective dose of natural radiation [3], and must not be neglected [4, 5]. In fact, worldwide studies suggest that under certain conditions, the annual equivalent lung dose of thoron can even exceed that of radon [6, 7, 8, 9, 10, 11]. In contrast to radon, the gas concentration of the short lived ^{220}Rn isotope (half-life $\tau_{1/2} = 55.6\ s$) is difficult to measure and advanced methods have to be applied [12]. It also has been pointed out, that passive sampling radon monitors may also be sensitive to thoron exposure, thus overestimating the radon exposure [13, 14, 15]. Recent developments already combine radon and thoron gas measurements [16, 17]. However, the devices are not designed as personal exposure monitors, or do not allow on-line evaluation. The improved HMGU radon/thoron monitor [18] remedies these issues by allowing to determine the thoron gas concentration in parallel while still being compact, and thus can be carried in a pocket.

In this paper an Geant4 application is discussed which allows to predict the alpha particle energy spectra for different device geometries at different environmental conditions in radon and thoron environments by means of Monte-Carlo simulations. The calculations were verified by comparison with measured alpha particle spectra for two different housing geometries and different radon/thoron atmospheres.

2. Materials and Methods

2.1. Exposimeter

In this work a recently developed diffusion chamber type device was used [18], employing pin-photodiode detectors, and an electro-conductive sponge as filter. A

*Email: josef.irlinger@helmholtz-muenchen.de

filter is necessary since detectors without filter have the disadvantage that their calibration factor (CF) is dependent on the progeny deposition rates influenced by humidity, aerosol concentration, airflow and equilibrium factor of the enviroment [19, 20, 21]. With filter the problem is avoided since a filter applied to the inlets of the diffusion chamber grants only undisturbed diffusion of the inert radon and thoron gas [22, 23], and the counts generated by the alpha decays from radon or thoron and its progeny are proportional to the respective gas activity concentration. Due to its low dependence on environmental parameters, this method has also been set as default method by the recently released ISO standards [24] for passive devices.

2.1.1. Housing size

Two different chamber geometries were realized, which were also implemented in the Monte Carlo simulation. The internal dimensions of the diffusion chambers are:

- Geometry 1: 108 $mm \times 57\ mm \times 26\ mm$ (length × width × height)
- Geometry 2: 116 $mm \times 90.5\ mm \times 47\ mm$ (length × width × height)

The small housing (geometry 1) is a Hammond Electronics 27134PSLA enclosure while the larger housing (geometry 2) is a 26908PSLA aluminum case.

2.2. Calibration Chamber

For the measurements an aluminum box with the following specifications was used,

- Manufacturer: ROSE, Type: 012333180
- Dimensions: 18 $cm \times 23\ cm \times 33\ cm$ ($h \times w \times l$), Volume: 13.5 l

It features additionally a 200 mm fan at the inside top of the chamber, needed for thoron mixing, 3 BNC connectors for online readout of the exposure meters, 1 BNC input for voltage supply, and 4 tube-connectors which allow to attach external pumps, sources or reference devices.
As radon source a uranite rock, also commonly called pitchblende, was used. A gamma-spectrometric analysis of a 0.538 g sample showed a specific ^{226}Ra activity of $23.0 \pm 0.4\ Bq\ g^{-1}$. As thoron source thorium-containing lantern mantles were used. The specific ^{232}Th activity of a 29.2 g probe (mean of 10 mantles) was determined to be $47.98 \pm 0.77\ Bq\ g^{-1}$. Humidity was controlled via saturated salt solutions using potassium carbonate (K_2CO_3), to keep exhalation rates and thus activity concentrations within the calibration chamber constant.

2.3. Meteorology

The reference device, a Durridge Rad7, was externally connected with tubes to the calibration chamber and its flow rate was determined to be 650 $cm^3\ min^{-1}$, i.e. 0.65 $l\ min^{-1}$, in exact agreement with the value given in the user manual [25]. The ^{220}Rn levels determined by the Rad7 were corrected depending on the measurement setup, since the volume of the connecting tubes V and the flow rate q of the device determine the loss of thoron before it reaches the inlet of the Rad7. The activity concentration C at the inlet depends on the original thoron concentration C_0 in the chamber via Equation 1 [26],

$$C = C_0\ e^{-\lambda\ V\ /\ q} \tag{1}$$

where λ is the decay constant of ^{220}Rn ($0.748\ min^{-1}$), V the sampling tube volume, which was determined from a 121 cm pipe length with 4 mm diameter to be 15.2 cm^3, and q the flow rate of the Rad7 ($650\ cm^3\ min^{-1}$). Hence, with this setup about 98.3% of the original thoron gas reached the Rad7. Since the device was calibrated by the manufacturer with a sampling volume of 50 cm^3 [25], which leads to a higher thoron loss ($C = 0.944\ C_0$), the measured concentration values for ^{220}Rn were too high and thus corrected by a factor $f = 1.0174/1.0559 = 0.963$.
Humidity and temperature were logged by the Rad7 while the absolute pressure was recorded with a *testo 511* barometer, featuring an accuracy of $\pm 3\ hPa$.

3. Monte Carlo simulation

Monte Carlo simulations of ^{222}Rn monitors were performed already very early [27], including diffusion into the detector chamber, to calculate the calibration factor on a theoretical basis. Another approach used a SRIM-based transport code to simulate alpha particle spectra [28] in dry air, while a recent study employed Geant4 to investigate the effect of environmental changes on the calibration factor [29]. All these studies focused, however, on passive solid state nuclear track detectors (SSNTD) only and therefore did not allow comparison of simulated and measured alpha particle energy spectra. With the newly developed device presented here this was for the first time possible.

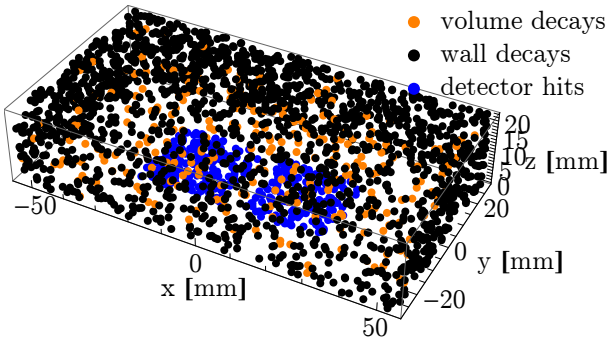

Figure 1: Schematic of employed simulation model showing origin of decays for geometry 1.

3.1. Simulation Model

The developed simulation is time-independent, which means diffusion processes were not taken into account and equilibrium between mother and daughter nuclides was assumed. For ^{222}Rn this is reached after about 7 h and for ^{220}Rn after about 70 h. Only the decay of alpha particle emitters is considered, i.e. $^{222}Rn \rightarrow {}^{218}Po \rightarrow {}^{214}Po$ for radon and $^{220}Rn \rightarrow {}^{216}Po \rightarrow {}^{212}Bi \rightarrow {}^{208}Tl$ and $^{212}Po \rightarrow {}^{208}Pb$ for thoron. For ^{222}Rn the activity ratio of the progeny is 1:1:1 and for ^{220}Rn 1:1:0.36:0.64 respectively. The alpha particle energies used in the simulation are stated in Table 1. Beta decays and δ-electrons were disregarded, since their deposited energies are in general way below the energy threshold of the detection system which is approximately 1 MeV. The alpha particles for radon and thoron gas were assumed to originate in the whole chamber volume, while the progeny alphas were assumed to originate from the wall and detector surfaces (except those from ^{216}Po), as illustrated in Figure 1. The deposition fraction of progeny on housing walls for cylindrical dimensions of up to 100 mm (height, diameter) is mostly > 0.9 for ^{218}Po and unity for ^{214}Po, ^{212}Po and ^{212}Bi [30], depending on the employed diffusion coefficient. For common detector geometries, which generally have a small volume, all deposition fractions are essentially equal to one [29]. All simulations performed in the framework of this work assume a unity deposition fraction for ^{218}Po, ^{214}Po, ^{212}Po and ^{212}Bi. The ^{216}Po progeny, with a half life of about 150 ms, has insufficient time for deposition on the surfaces, and it is more likely to decay within the volume. In conclusion the following nuclides were considered:

- ^{222}Rn, ^{220}Rn and ^{226}Po randomly decay, with respect to origin and direction, within the simulation volume as well as on volume and detector surfaces.
- ^{218}Po, ^{214}Po, ^{212}Bi and ^{212}Po randomly decay only on volume and detector surfaces.

Accordingly, ^{222}Rn and most of its progeny are therefore distributed via a uniform probability density function (PDF) within the volume and the surface. In contrast for thoron and its first progeny (^{216}Po), which immediately follows its decay, the diffusion length L has to be considered, as the concentration decreases exponentially from the entry point. The simulation also considers the energy loss of alpha particles at the 400 nm aluminum cover of the detectors.
In order to define the direction of alpha particles produced during decay of radon, thoron, and their progeny, arbitrary polar angles θ and azimuthal angle ϕ were generated by choosing u and v to be random variates on [0,1], with $\phi = 2\,\pi\,u$ and $\theta = cos^{-1}(2\,v - 1)$. In the simulation only alpha particles moving towards the detectors were considered.

3.2. Particle Transport Code

Within the framework of this work the Geant4 toolkit (version 9.5.2) was employed, which is an open source C++ code, originally developed for high energy physics [34]. For validating the Geant4 calculations an analytic simulation relying on the NIST alpha stopping power and range (ASTAR) database [35] was developed, which itself is a program based on the ICRU 49 report [36], and implemented in Wolfram Mathematica. A comparison of simulation results obtained with both methods at standard temperature and pressure (STP) conditions yielded similar results (4% to 13% deviation of the calculated calibration factor).

3.3. Air Composition

The composition of air, including its most important constituents, is, for example, defined by the National Institute of Standards and Technology (NIST) at 0% relative humidity (RH), 20 $^{\circ}C$ and $1,013.25$ hPa, with a density of 1.20479 $mg\ cm^{-3}$ at STP . Dalton's law of partial pressure was applied to calculate the air composition with water vapor (considering only elements C, Ar, N, O and H), depending on temperature, pressure and RH. The saturation vapor pressure was calculated via the Goff-Gratch equation [37]. Another parameter needed in Geant4 to simulate the energy loss of alpha particles in air is its density. The ideal gas law $pV = nRT$, combined with Dalton's law, yields Equation 2 for the calculation of the air density ρ,

$$\rho = \frac{p_{air}\ M_{air}}{R\ T} + \frac{p_{water}\ M_{water}}{R\ T} \tag{2}$$

where M_{index} is the molecular mass of the respective gas.

Table 1: Radon/Thoron decay series properties

Nuclide	Half-Life[1]	E_α [1] (MeV)	$\sum E_\alpha(PAE)\ (MeV)$	rel. EEC[2]
^{222}Rn	3.82 d	5.59	19.53	-
^{218}Po	3.10 min	6.11	13.94	0.105
^{214}Pb	26.8 min	-	7.83	0.516
^{214}Bi	19.9 min	-	7.83	0.379
^{214}Po	164.3 μs	7.83	7.83	0.00
^{210}Pb	22.2 a	-	-	-
^{220}Rn	55.6 s	6.40	21.27	-
^{216}Po	145 ms	6.91	14.87	0.00
^{212}Pb	10.64 h	-	7.96	0.913
^{212}Bi	60.6 min	6.21	7.96	0.087
^{212}Po	299 ns	8.95	5.73	0.00

[1] [31, 32], [2] [33]

3.4. Factor to compare Simulation and Measurement

The normalization factor needed to compare simulated and measured alpha particle spectra depends on the total count number ct (measured or simulated in the sensitive detector volume) and the decays N that actually occurred or were simulated in the housing of the detector. If all other relevant parameters are correctly considered in the simulation, one will be able to model the measurement conditions realistically. Then the ratio of the measured count number ct_m and the number of total actual decays (N_{actual}) is the same as that of the simulated count number (ct_s) and the number of total decays in the simulation (N_{sim}).

$$\frac{ct_m}{N_{actual}} = \frac{ct_s}{N_{sim}} \tag{3}$$

where ct_m and ct_s are the counts actually measured or scored on the detector surface in the simulation. The total number N_{actual} of airborne ^{222}Rn or ^{220}Rn decays in Equation 3 can be estimated from the measured reference activity concentration $C(t)$ via,

$$N_{actual} = V \int_0^{t_m} C(t)\, dt \tag{4}$$

where V is the inner housing volume of the exposimeter and t_m the measurement time. Hence, according to Equation 3 a simulated spectrum needs to be multiplied by N_{actual}/N_{sim}, when comparing with a measured spectra, where N_{actual} is calculated via Equation 4.

3.5. Enegery Spectra Dependence on Electronics

The histogram of all counts scored on the detector surface versus the energies deposited in the detector, yields a simulated spectrum with a discrete number of energies. In order to achieve a better agreement between simulation and measurement, however, one has to consider the energy broadening introduced by the amplification stage. This is generally done by applying the Gaussian energy broadening (GEB) method [38], via multiplication of each individual energy bin value with a normalized Gaussian function. The standard deviation σ of the applied Gaussian, is related to the $FWHM$ energy resolution ΔE of the detector system via $\Delta E = 2\sqrt{2\ln 2}\,\sigma$. The energy resolution of the system was experimentally determined to be $\Delta E = 200\ keV$ for Geo1 and $\Delta E = 150\ keV$ for Geo2. The energy threshold has been set to 1 MeV.

3.6. Calibration Factor

The calibration factor obtained from a simulation, depends on the events, the volume and the registered count number. The simulated activity concentration C_s is given by,

$$C_s = \frac{N_{sim}}{V\ t} \tag{5}$$

where the time interval t can be chosen freely for any $t > 0$, since the simulation is time independent. The simulated observed counts ct_s are assigned the unit counts per time interval (cpt). The calibration factor cf from simulation results is then calculated according to Equation 6,

$$cf_{sim} = \frac{C_s}{ct_s} = \frac{N_{sim}}{V\ t\ ct_s} \tag{6}$$

In the following t is chosen to be 3600 seconds for ease of comparison, which yields a calibration factor unit of $Bq\ m^{-3}/cph$. In all the results presented the number of simulated decays was $1.5 \cdot 10^5$ directed into the 2π solid

angle towards the detectors, which equals an actual decay number of $N_{sim} = 3 \cdot 10^5$ when considering the 4π solid angle.

4. Results and Discussion

4.1. Spectral Comparison

4.1.1. Measurement in pure Radon Atmosphere

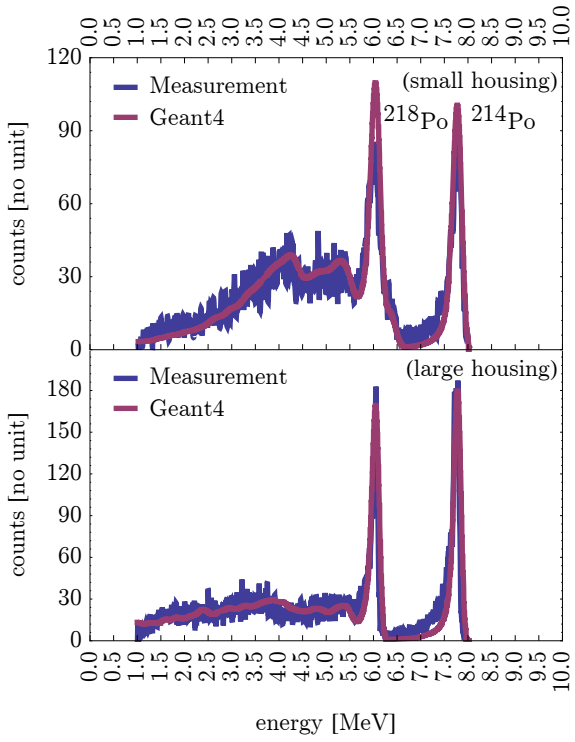

Figure 2: Simulated and measured spectra in a ^{222}Rn environment for geometries 1 (small housing) and 2 (large housing).

Several calibration measurements at laboratory conditions were performed. Temperature and pressure were not controlled but continuously monitored. Figure 2 shows two typical alpha particle spectra for the two different geometries in a ^{222}Rn environment. The mean environmental conditions during the calibration period (between hour 85 to 115 after having closed the calibration chamber) were 45% RH, 16.3 $^{\circ}C$ and 968.4 hPa. The mean ^{222}Rn concentration was $6,866 \pm 331$ $Bq\ m^{-3}$ while only negligible ^{220}Rn was present (7 ± 27 $Bq\ m^{-3}$), both concentrations measured by the reference device. The total exposure due to ^{222}Rn was $212,830 \pm 1,845$ $Bq\ h\ m^{-3}$. Geometry 1 had a volume of 124.4 cm^3 and geometry 2 of about 493.4 cm^3. The number of decays N that occurred during the measurement within the respective volume and the given ^{222}Rn concentration, were are $N_{actual,geo1} = 122,633$ and $N_{actual,geo2} = 378,042$, respectively (Eq. 4). The normalization factor for comparing measurement and simulation was calculated via Equation 3, and the resulting total number of measured and simulated counts as a function of energy are shown in Figure 2. Energy calibration was performed by evaluating the channel number of the clearly visible progeny peaks, assigning the energy according to the simulated value, and assuming a linear energy-channel relationship.
Figure 2 demonstrates a reasonable agreement between measurement and simulation, both in terms of absolute counts per channel as well as energy dependence. This is particularly noteworthy because the simulation was not adjusted via any least-squares fit, but only via Equation 3, where the number of simulated events was $N_{sim} = 3 \cdot 10^5$, and $N_{actual,geo1}$ and $N_{actual,geo2}$ as given above. This indicates that the most important factors influencing the shape and count number of the acquired spectrum have been considered in the simulation.

Table 2 shows the count number for the two geometries and corresponding pressures values of the simulated alpha particle energy spectra shown in Figure 2. The total count number results from the integration over the number of registered events. The main contribution to the total count number was from airborne ^{222}Rn decays in the detector housing, for both devices (about 40%). The total number of scored particles, which enter the sensitive detector volume, is smaller in case of the larger housing. The reason is the static number of simulated events, which results for a larger volume into a decreased concentration C_s (Eq. 5). In both cases the statistical uncertainty is well below 1%.

4.1.2. Measurement in pure Thoron Atmosphere

In principle the simulation of ^{220}Rn is similar to that of ^{222}Rn except for the difference in the isotope diffusion length in steady air, which is $L \approx 3.0$ cm for thoron as compared to $L \approx 2.20$ m for radon [39]. More specifically, the activity concentration of radon or thoron decreases exponentially with distance z from the inlet area with $C(z) = C_0\ e^{-z/L}$ [40], where C_0 is the activity concentration at zero distance from the inlet. In Figure 3 two measured spectra are compared with the corresponding simulated spectra, for the two available housing geometries. The small housing (Geo1) alpha particle spectrum was acquired at 46% RH, 23.4 $^{\circ}C$ and 968.6 hPa (between hours 60-77 after having closed the

Table 2: Individual radon contributions to the simulated spectra of Figure 2, for the small and large housing.

Geometry	Nuclide	^{222}Rn	^{218}Po	^{214}Po	Sum
small	counts	16,040	11,765	12,262	40,067
	fraction	0.40	0.29	0.31	1
large	counts	5,507	3,478	5,222	14,206
	fraction	0.39	0.24	0.37	1

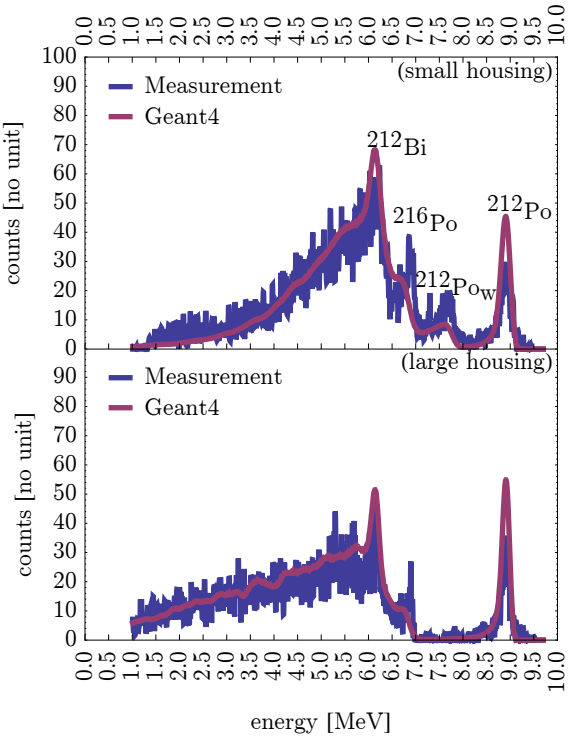

Figure 3: Simulated and measured alpha particle spectra in a ^{220}Rn environment for geometries 1 (small) and 2 (large).

calibration chamber) at a mean activity concentration of $8,263 \pm 332$ $Bq\ m^{-3}$ for ^{220}Rn and 91 ± 130 $Bq\ m^{-3}$ for ^{222}Rn, both again measured by the reference device. The exposure due to thoron was thus about $148,724 \pm 331$ $Bq\ h\ m^{-3}$ resulting in estimated decays that occurred in the measurement chamber during that time of $N_{actual,geo1} = 85,695$. Accordingly, the spectra for the larger housing (Geo2) was acquired during hours 60-85 at 44% RH, 24.2 $°C$, 961.0 hPa and a mean ^{220}Rn concentration of $3,916 \pm 259$ $Bq\ m^{-3}$ (^{222}Rn: 69 ± 117 $Bq\ m^{-3}$). The thoron exposure measured by the reference device was $101,811 \pm 1323$ $Bq\ h\ m^{-3}$ and therefore $N_{actual,geo2} = 180,842$. The corresponding measured and simulated alpha particle spectra shown in Figure 3, again agree well, as was the case in Figure 2 for the ^{222}Rn environment. A closer look reveals, however, that the ^{216}Po progeny peak actually measured is higher than expected from the simulation, while the ^{212}Po peak is lower and the measured $^{212}Po_w$ peak (progeny decays originating from the volume inner surfaces, where index w stands for *wall*) is higher. The reason for this is most probably the complex diffusion behavior of decay products, which is not considered in the static simulation. Nevertheless, both the energy position of the peaks and their amplitudes were simulated reasonably well. Further, one can recognize some measured counts beyond the right edge of the ^{212}Po peak at about 9.16 MeV. These counts originate from pile-ups due to e^- from the β^- decay (2.25 MeV) of ^{212}Bi which is directly followed by a ^{212}Po alpha decay ($\tau_{1/2} = 298$ ns), which was also not considered in the simulation.

4.2. Calibration Factors

The characteristic quantity of a radon monitor is its calibration factor, which can be calculated via Equation 6. The calibration factor calculated from a simulation is completely independent of any reference concentration measurements. The number of simulated counts ct_s is integrated from 1 to 10 MeV, using the same energy bin widths as defined by the corresponding measurement. For geometry 1 the measured calibration factor was $cf_{meas} = 16.9 \pm 0.2$ $Bq\ m^{-3}/cph$ (mean±std) which is very close the simulated one of $cf_{sim} = 16.8 \pm 0.7$ $Bq\ m^{-3}/cph$, where the given uncertainty was calculated via Gaussian error propagation, assuming an uncertainty of 1 mm for all geometric dimensions. For geometry 2 the corresponding calibration factors were cf_{meas} of 11.3 ± 0.5 $Bq\ m^{-3}/cph$ and cf_{sim} of 10.7 ± 0.3 $Bq\ m^{-3}/cph$. The relative differences between the measured and simulated values are hence about 1% and 6%, respectively, which is considered acceptable.

4.3. Measurement in mixed Radon/Thoron Atmospheres

One potential application of the simulated alpha particle energy spectra is to use them in evaluating results obtained in mixed radon/thoron environments. The

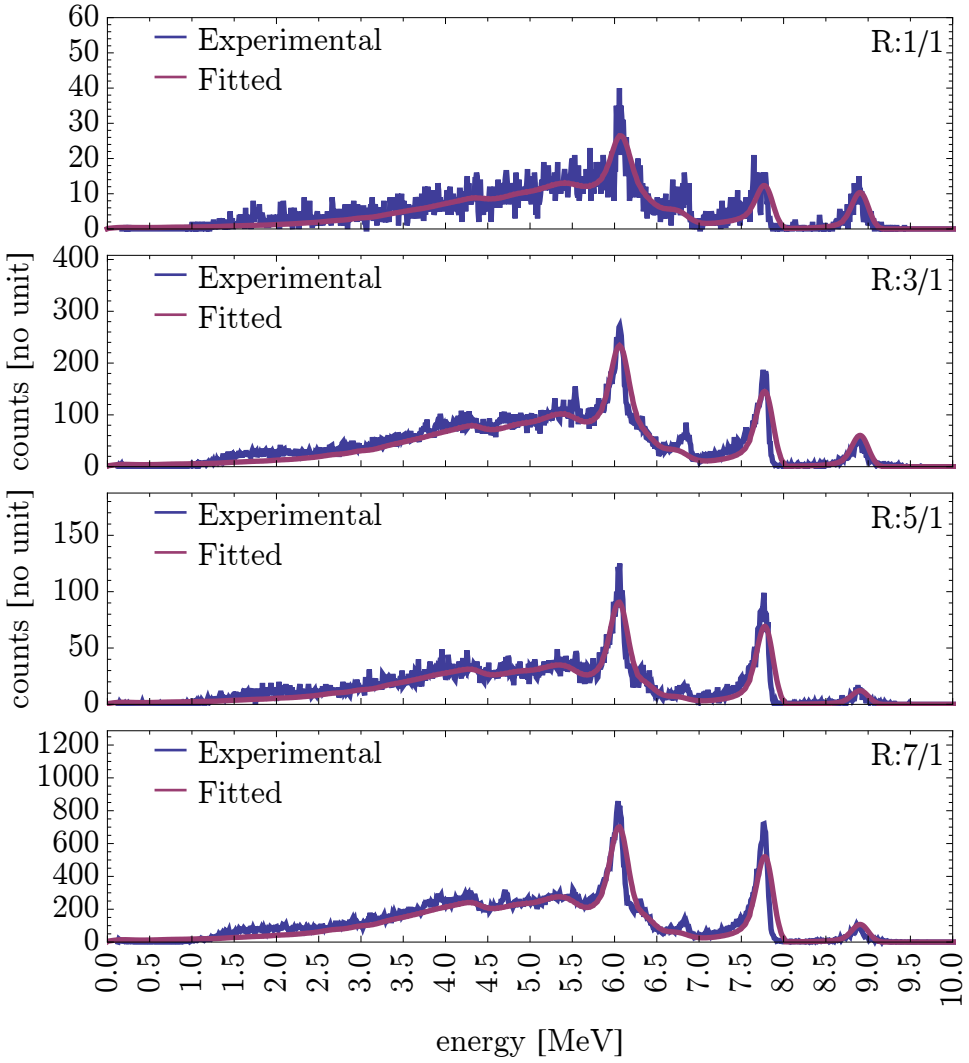

Figure 4: Experimentally acquired spectra in mixed ^{222}Rn and ^{220}Rn concentrations and fits of linear combinations of normalized simulated spectra. "R: rn/tn" indicates the ratio of radon to thoron concentration. Trend shows good agreement, however, calculated concentrations differ somewhat (see Table 3).

method described here employs a least square approximation, where the fitting parameters are the constants of a linear combination of normalized spectra simulated for radon and thoron. Under ideal conditions any spectrum acquired ($\mathbf{S}_{meas}$) in a $^{222}Rn/^{220}Rn$ mixed atmosphere should be just a linear combination of a radon and a thoron spectrum $\mathbf{S}_i^N$, both obtained in a reference simulation, and each weighted with an appropriate factor a, b (Eq. 7).

$$\mathbf{S}_{meas} = a\,\mathbf{S}^N_{^{222}Rn} + b\,\mathbf{S}^N_{^{220}Rn} \tag{7}$$

Note that this is only true if the environmental conditions such as air pressure during the measurement in a mixed atmosphere is similar to those under reference conditions. Figure 4 shows four spectra measured in mixed radon/thoron atmospheres and the corresponding linear combinations of simulated radon and thoron spectra. The fitting procedure employed was *LinearModelFit* of *Wolfram Mathematica 9.0.1*, using weights $w_x = 1/u(x)$ for each channel x, where the error $u(x) = \sqrt{ct_x}$ is taken to be the statistical uncertainty. Comparing the trend of spectral form and the absolute count number per channel between measured and fitted spectrum in Figure 4, one notes a reasonable agreement for all four measurements. The values of the activity concentrations found with this method, however, show some deviations from the reference mean values, determined with the reference device.

The difference between the values found by the fitting method and the reference concentrations (Table 3) is most likely due to the fact that the fitting procedure does not yet include appropriate weighting factors reflecting the importance of certain energy regions of the two radon/thoron spectra. Nevertheless, even in mixed atmospheres where thoron cannot be ignored compared to radon, reasonable results within about 30% were already obtained.

5. Conclusion

For the first time, the Geant4 Monte-Carlo toolkit was used to simulate alpha particle energy spectra measured in ^{222}Rn and ^{220}Rn atmospheres with the new HMGU radon/thoron electronic exposimeter. Results obtained with Geant4 were validated by means of analytic calculations based on state-of-the-art stopping power data. Furthermore, it was shown that a simple static model, taking only alpha particle decays into account and assuming a homogenous progeny distribution within the detector housing, is sufficient to obtain reasonable agreement between simulated and measured alpha particle spectra and calibration factors for both ^{222}Rn and ^{220}Rn atmospheres. It was demonstrated that the simulated alpha particle energy spectra can be used to interpret alpha particle energy spectra obtained in mixed radon/thoron atmospheres. The Geant4 simulations can now be utilized to systematically study the dependence of the calibration factors for both ^{222}Rn and ^{220}Rn on environmental parameters such as relative humidity, ambient temperature and pressure.

References

[1] F. L. Karinda, B. Haider, W. Rühm, A new electronic personal exposure meter for radon gas, Radiation Measurements 43 (2–6) (2008) 1170–1174, ISSN 1350-4487, doi:\bibinfo{doi}{10.1016/j.radmeas.2007.10.012}, URL http://www.sciencedirect.com/science/article/pii/S1350448707004039.

[2] E. Gruber, E. Salama, W. Rühm, Real-time measurement of individual occupational radon exposures in tombs of the Valley of the Kings, Egypt, Radiation Protection Dosimetry 144 (1-4) (2011) 620–626, ISSN 0144-8420, 1742-3406, doi:\bibinfo{doi}{10.1093/rpd/ncq450}, URL http://rpd.oxfordjournals.org/content/144/1-4/620.

[3] UNSCEAR, UNSCEAR 2008 Report, Vol. I: Sources of ionizing radiation. Annex A: Medical Radiation Exposures, New York, NY: United Nations, 2010.

[4] F. Steinhäusler, W. Hofmann, H. Lettner, Thoron Exposure of Man: A Negligible Issue?, Radiation Protection Dosimetry 56 (1-4) (1994) 127–131, ISSN 0144-8420, 1742-3406, URL http://rpd.oxfordjournals.org/content/56/1-4/127.

[5] S. Tokonami, Why is 220Rn (thoron) measurement important?, Radiation Protection Dosimetry 141 (4) (2010) 335–339, ISSN 0144-8420, 1742-3406, doi:\bibinfo{doi}{10.1093/rpd/ncq246}, URL http://rpd.oxfordjournals.org/content/141/4/335.

[6] J. Tschiersch, W. B. Li, O. Meisenberg, Increased indoor thoron concentrations and implication to inhalation dosimetry, Radiation Protection Dosimetry 127 (1-4) (2007) 73–78, ISSN 0144-8420, 1742-3406, doi:\bibinfo{doi}{10.1093/rpd/ncm341}, URL http://rpd.oxfordjournals.org/content/127/1-4/73.

[7] O. Meisenberg, J. Tschiersch, Thoron in indoor air: modeling for a better exposure estimate, Indoor Air 21 (3) (2011) 240–252, ISSN 1600-0668, doi:\bibinfo{doi}{10.1111/j.1600-0668.2010.00697.x}, URL http://onlinelibrary.wiley.com/doi/10.1111/j.1600-0668.2010.00697.x/abstract.

[8] J. Wiegand, S. Feige, X. Quingling, U. Schreiber, K. Wieditz, C. Wittmann, L. Xiarong, Radon and thoron in cave dwellings (Yan'an, China), Health Physics 78 (4) (2000) 438–444, URL http://journals.lww.com/health-physics/Abstract/2000/04000/Radon_and_Thoron_in_Cave_Dwellings__Yan_an,_China_.8.aspx.

[9] M. Sreenath Reddy, P. Yadagiri Reddy, K. Rama Reddy, K. P. Eappen, T. V. Ramachandran, Y. S. Mayya, Thoron levels in the dwellings of Hyderabad city, Andhra Pradesh, India, Journal of Environmental Radioactivity 73 (1) (2004) 21–28, ISSN 0265-931X, doi:\bibinfo{doi}{10.1016/j.jenvrad.2003.07.002}, URL http://www.sciencedirect.com/science/article/pii/S0265931X03002236.

Table 3: Ratio R of ^{222}Rn and ^{220}Rn concentrations based on reference measurements, and single radon and thoron concentrations measured or fitted (see Fig. 4).

Ratio	Radon $[Bq/m^3]$		Thoron $[Bq/m^3]$	
	Reference	Fit	Reference	Fit
1/1	1150 ± 210	960 ± 40	1480 ± 110	1360 ± 30
3/1	17730 ± 630	11800 ± 220	5980 ± 350	7920 ± 200
5/1	6300 ± 300	5770 ± 100	1260 ± 100	1600 ± 90
7/1	65960 ± 1190	43220 ± 710	9050 ± 510	14090 ± 650

[10] B. Shang, J. Tschiersch, H. Cui, Y. Xia, Radon survey in dwellings of Gansu, China: the influence of thoron and an attempt for correction, Radiation and Environmental Biophysics 47 (3) (2008) 367–373, ISSN 0301-634X, 1432-2099, doi:\bibinfo{doi}{10.1007/s00411-008-0163-2}, URL http://link.springer.com/article/10.1007/s00411-008-0163-2.

[11] J. McLaughlin, M. Murray, L. Currivan, D. Pollard, V. Smith, S. Tokonami, A. Sorimachi, M. Janik, Long-term measurements of thoron, its airborne progeny and radon in 205 dwellings in Ireland, Radiation Protection Dosimetry 145 (2-3) (2011) 189–193, ISSN 0144-8420, 1742-3406, doi:\bibinfo{doi}{10.1093/rpd/ncr067}, URL http://rpd.oxfordjournals.org/content/145/2-3/189.

[12] C. Nuccetelli, F. Bochicchio, The Thoron Issue: Monitoring Activities, Measuring Techniques and Dose Conversion Factors, Radiation Protection Dosimetry 78 (1) (1998) 59–64, ISSN 0144-8420, 1742-3406, URL http://rpd.oxfordjournals.org/content/78/1/59.

[13] D. Nikezić, K. N. Yu, The influence of thoron and its progeny on radon measurements with CR39 detectors in diffusion chambers, Nuclear Instruments and Methods in Physics Research Section A: Accelerators, Spectrometers, Detectors and Associated Equipment 419 (1) (1998) 175–180, ISSN 0168-9002, doi:\bibinfo{doi}{10.1016/S0168-9002(98)01152-8}, URL http://www.sciencedirect.com/science/article/pii/S0168900298011528.

[14] S. Tokonami, M. Yang, T. Sanada, CONTRIBUTION FROM THORON ON THE RESPONSE OF PASSIVE RADON DETECTORS, Health Physics 80 (6) (2001) 612–615, ISSN 0017-9078, URL http://ovidsp.ovid.com/ovidweb.cgi?T=JS&CSC=Y&NEWS=N&PAGE=fulltext&D=yrovfte&AN=00004032-200106000-00014.

[15] C. G. Sumesh, A. Vinod Kumar, R. M. Tripathi, R. N. Nair, V. D. Puranik, Impact of flow rate on sensitivity of semiconductor type thoron monitor, Radiation Measurements 59 (2013) 241–244, ISSN 1350-4487, doi:\bibinfo{doi}{10.1016/j.radmeas.2013.07.007}, URL http://www.sciencedirect.com/science/article/pii/S1350448713002886.

[16] S. Tokonami, M. Yang, H. Yonehara, Y. Yamada, Simple, discriminative measurement technique for radon and thoron concentrations with a single scintillation cell, Review of Scientific Instruments 73 (1) (2002) 69–72, ISSN 0034-6748, 1089-7623, doi:\bibinfo{doi}{10.1063/1.1416121}, URL http://scitation.aip.org/content/aip/journal/rsi/73/1/10.1063/1.1416121.

[17] S. Tokonami, H. Takahashi, Y. Kobayashi, W. Zhuo, E. Hulber, Up-to-date radon-thoron discriminative detector for a large scale survey, Review of Scientific Instruments 76 (11) (2005) 113505, ISSN 0034-6748, 1089-7623, doi:\bibinfo{doi}{10.1063/1.2132270}, URL http://scitation.aip.org/content/aip/journal/rsi/76/11/10.1063/1.2132270.

[18] J. Irlinger, M. Wielunski, W. Rühm, Thoron detection with an active Radon exposure meter—First results, Review of Scientific Instruments 85 (2) (2014) 022106, ISSN 0034-6748, 1089-7623, doi:\bibinfo{doi}{10.1063/1.4865162}, URL http://scitation.aip.org/content/aip/journal/rsi/85/2/10.1063/1.4865162.

[19] D. Arnold, K. N. Yu, Uncertainty in radon measurements with CR39 detector due to unknown deposition of 218Po, Nuclear Instruments and Methods in Physics Research Section A: Accelerators, Spectrometers, Detectors and Associated Equipment 450 (2–3) (2000) 568–572, ISSN 0168-9002, doi:\bibinfo{doi}{10.1016/S0168-9002(00)00309-0}, URL http://www.sciencedirect.com/science/article/pii/S0168900200003090.

[20] D. Nikezic, K. N. Yu, Computer simulation of radon measurements with nuclear track detectors, Computer physics research trends 3 (2007) 119–150, URL http://www.cityu.edu.hk/ap/nru/CPRT.pdf.

[21] R. Mishra, Y. S. Mayya, Study of a deposition-based direct thoron progeny sensor (DTPS) technique for estimating equilibrium equivalent thoron concentration (EETC) in indoor environment, Radiation Measurements 43 (8) (2008) 1408–1416, ISSN 1350-4487, doi:\bibinfo{doi}{10.1016/j.radmeas.2008.03.002}, URL http://www.sciencedirect.com/science/article/pii/S1350448708000838.

[22] Y. Yoshtoa, K. Kitano, . Murata, S. Moriyasu, Comparison of performance characteristics of some filters using Thoron daughters as radioactive aerosol URL http://www.irpa.net/irpa1/cdrom/VOL.2/R2_94.PDF.

[23] R. G. Stafford, H. J. Ettinger, Filter efficiency as a function of particle size and velocity, Atmospheric Environment (1967) 6 (5) (1972) 353–362, ISSN 0004-6981, doi:\bibinfo{doi}{10.1016/0004-6981(72)90201-6}, URL http://www.sciencedirect.com/science/article/pii/0004698172902016.

[24] ISO, ISO 11665-5:2012 - Measurement of radioactivity in the environment – Air: radon-222 – Part 5: Continuous measurement method of the activity concentration, no. 5 in 11665, International Organization for Standardization, URL http://www.iso.org/iso/home/news_index/news_archive/news.htm?refid=Ref1684, 2012.

[25] Durridge, RAD7 RADON DETECTOR User Manual, URL http://www.durridge.com/documentation/RAD7%20Manual.pdf, 2014.

[26] A. Sorimachi, T. Ishikawa, M. Janik, S. Tokonami, Quality assurance and quality control for thoron measurement at NIRS, Radiation Protection Dosimetry 141 (4) (2010) 367–370, ISSN 0144-8420, 1742-3406, doi:\bibinfo{doi}{10.1093/rpd/ncq245}, URL http://rpd.oxfordjournals.org/content/141/4/367.

[27] M. Urban, Passive one-element track etch dosemeter for simultaneous measurement of radon, thoron and decay prod-

ucts in air, International Journal of Radiation Applications and Instrumentation. Part D. Nuclear Tracks and Radiation Measurements 12 (1–6) (1986) 685–688, ISSN 1359-0189, doi:\bibinfo{doi}{10.1016/1359-0189(86)90679-5}, URL http://www.sciencedirect.com/science/article/pii/1359018986906795.

[28] J. Rickards, J.-I. Golzarri, G. Espinosa, A Monte Carlo study of radon detection in cylindrical diffusion chambers, Journal of Environmental Radioactivity 101 (5) (2010) 333–337, ISSN 0265-931X, doi:\bibinfo{doi}{10.1016/j.jenvrad.2010.01.003}, URL http://www.sciencedirect.com/science/article/pii/S0265931X10000184.

[29] C. Zhao, W. Zhuo, D. Fan, Y. Yi, B. Chen, Effects of atmospheric parameters on radon measurements using alpha-track detectors, Review of Scientific Instruments 85 (2) (2014) 022101, ISSN 0034-6748, 1089-7623, doi:\bibinfo{doi}{10.1063/1.4865155}, URL http://scitation.aip.org/content/aip/journal/rsi/85/2/10.1063/1.4865155.

[30] D. Pressyanov, I. Rusinov, G. Simeonov, Radon progeny deposition in track-detection diffusion chambers, Nuclear Instruments and Methods in Physics Research Section A: Accelerators, Spectrometers, Detectors and Associated Equipment 435 (3) (1999) 509–513, ISSN 0168-9002, doi:\bibinfo{doi}{10.1016/S0168-9002(99)00578-1}, URL http://www.sciencedirect.com/science/article/pii/S0168900299005781.

[31] K. Eckerman, A. Endo, ICRP Publication 107. Nuclear decay data for dosimetric calculations., Annals of the ICRP 38 (3) (2007) 7–96, URL http://europepmc.org/abstract/MED/19285593.

[32] R. B. Firestone, The Berkeley Laboratory Isotopes Project, URL http://ie.lbl.gov/education/isotopes.htm, 2000.

[33] UNSCEAR, Effects of Ionizing Radiation: United Nations Scientific Committee on the Effects of Atomic Radiation-UNSCEAR 2006 Report, Volume II-Report to the General Assembly, with Scientific Annexes C, D, and E, vol. 2, United Nations Publications, URL http://www.unscear.org/unscear/en/publications/2006_2.html, 2009.

[34] S. Agostinelli, J. Allison, K. Amako, J. Apostolakis, H. Araujo, P. Arce, M. Asai, D. Axen, S. Banerjee, G. Barrand, F. Behner, L. Bellagamba, J. Boudreau, L. Broglia, A. Brunengo, H. Burkhardt, S. Chauvie, J. Chuma, R. Chytracek, G. Cooperman, G. Cosmo, P. Degtyarenko, A. Dell'Acqua, G. Depaola, D. Dietrich, R. Enami, A. Feliciello, C. Ferguson, H. Fesefeldt, G. Folger, F. Foppiano, A. Forti, S. Garelli, S. Giani, R. Giannitrapani, D. Gibin, J. J. Gómez Cadenas, I. González, G. Gracia Abril, G. Greeniaus, W. Greiner, V. Grichine, A. Grossheim, S. Guatelli, P. Gumplinger, R. Hamatsu, K. Hashimoto, H. Hasui, A. Heikkinen, A. Howard, V. Ivanchenko, A. Johnson, F. W. Jones, J. Kallenbach, N. Kanaya, M. Kawabata, Y. Kawabata, M. Kawaguti, S. Kelner, P. Kent, A. Kimura, T. Kodama, R. Kokoulin, M. Kossov, H. Kurashige, E. Lamanna, T. Lampén, V. Lara, V. Lefebure, F. Lei, M. Liendl, W. Lockman, F. Longo, S. Magni, M. Maire, E. Medernach, K. Minamimoto, P. Mora de Freitas, Y. Morita, K. Murakami, M. Nagamatu, R. Nartallo, P. Nieminen, T. Nishimura, K. Ohtsubo, M. Okamura, S. O'Neale, Y. Oohata, K. Paech, J. Perl, A. Pfeiffer, M. G. Pia, F. Ranjard, A. Rybin, S. Sadilov, E. Di Salvo, G. Santin, T. Sasaki, N. Savvas, Y. Sawada, S. Scherer, S. Sei, V. Sirotenko, D. Smith, N. Starkov, H. Stoecker, J. Sulkimo, M. Takahata, S. Tanaka, E. Tcherniaev, E. Safai Tehrani, M. Tropeano, P. Truscott, H. Uno, L. Urban, P. Urban, M. Verderi, A. Walkden, W. Wander, H. Weber, J. P. Wellisch, T. Wenaus, D. C. Williams, D. Wright, T. Yamada, H. Yoshida, D. Zschiesche, Geant4—a simulation toolkit, Nuclear Instruments and Methods in Physics Research Section A: Accelerators, Spectrometers, Detectors and Associated Equipment 506 (3) (2003) 250–303, ISSN 0168-9002, doi:\bibinfo{doi}{10.1016/S0168-9002(03)01368-8}, URL http://www.sciencedirect.com/science/article/pii/S0168900203013688.

[35] M. J. Berger, J. S. Coursey, M. A. Zucker, J. Chang, Stopping-power and range tables for electrons, Positrons, and Helium Ions .

[36] H. Paul, The Stopping Power of Matter for Positive Ions, Johannes Kepler University Linz URL http://cdn.intechopen.com/pdfs/34244.pdf.

[37] D. M. Murphy, T. Koop, Review of the vapour pressures of ice and supercooled water for atmospheric applications, Quarterly Journal of the Royal Meteorological Society 131 (608) (2005) 1539–1565, ISSN 1477-870X, doi:\bibinfo{doi}{10.1256/qj.04.94}, URL http://onlinelibrary.wiley.com/doi/10.1256/qj.04.94/abstract.

[38] X. G. Xu, K. F. Eckerman, Handbook of Anatomical Models for Radiation Dosimetry, CRC Press, ISBN 978-1-4200-5980-9, 2009.

[39] A. K. Narula, S. K. Goyal, S. Saini, R. P. Chauhan, S. K. Chakarvarti, Calculation of radon diffusion coefficient and diffusion length for different building construction materials, Indian Journal of Physics 83 (8) (2009) 1171–1175, doi:\bibinfo{doi}{10.1007/s12648-009-0097-9}.

[40] J. McLaughlin, An overview of thoron and its progeny in the indoor environment, Radiation Protection Dosimetry 141 (4) (2010) 316–321, ISSN 0144-8420, 1742-3406, doi:\bibinfo{doi}{10.1093/rpd/ncq234}, URL http://rpd.oxfordjournals.org/content/141/4/316.